

Quantum diatomic chain: a supersolid structure in three-component Bose mixture

Francesco Ancilotto^{1,2}

¹*Dipartimento di Fisica e Astronomia “Galileo Galilei” and CNISM,
Università di Padova, via Marzolo 8, 35122 Padova, Italy*

²*CNR-Istituto Officina dei Materiali (IOM), via Bonomea, 265 - 34136 Trieste, Italy
(Dated: December 19, 2025)*

The formation and properties of a supersolid structure in a three-component ultracold Bose gas mixture at $T=0$ are investigated theoretically. The system consists of ^{23}Na , ^{39}K , and ^{41}K atomic species, in which the binary mixtures of (^{23}Na , ^{39}K) and (^{39}K , ^{41}K) can form self-bound quantum droplets stabilized by quantum fluctuations. Two such droplets can bind together by the shared ^{39}K component, forming a stable “dimer” structure, which displays vibrational modes analogous to a classical diatomic molecule. A simple protocol is proposed to create a stable linear chain formed by periodic repetition of this basic building block, i.e. an alternating sequence of (^{23}Na , ^{39}K) and (^{39}K , ^{41}K) droplets. This structure exhibits both periodic density modulations from the droplet ordering and global phase coherence due to the shared ^{39}K component, satisfying the criteria for supersolidity. This expands the class of known supersolids by adding a system where mediated binding — rather than intrinsic long-range interactions or engineered band-structures as in previously known supersolids — is the key organizing principle, thereby offering new directions for both theory and experiment. The low-energy excitation spectrum, probed by density perturbations, identifies modes corresponding to droplet vibrations close to the ones expected from a classical diatomic chain, coexisting with low-energy superfluid (Goldstone-type) modes.

I. INTRODUCTION

The study of ultracold quantum gases has been at the forefront of atomic, molecular, and optical physics for decades now, often unveiling new states of matter and quantum phenomena [1–4]. Among the fascinating phenomena observed in these systems, quantum droplets and supersolids have gained significant attention due to their unique properties and potential for advancing our understanding of quantum matter.

Quantum droplets were first predicted theoretically by Petrov in 2015 [5] and subsequently observed experimentally in dipolar gases [6–9] as well as in homonuclear [10, 11] and heteronuclear [12, 13] mixtures. These self-bound states are stabilized by quantum fluctuations, typically described by the Lee-Huang-Yang (LHY) correction [14], which counteracts the mean-field attraction that would otherwise lead to collapse. Quantum droplets are self-bound states characterized by ultralow equilibrium densities and surface tension. These droplets exhibit liquid-like properties while maintaining quantum coherence, making them a unique form of matter that bridges the gap between classical liquids and quantum gases.

Supersolidity, a paradoxical state of matter combining the seemingly contradictory properties of crystalline order and frictionless flow, was first proposed by Andreev and Lifshitz in 1969 [15] and Leggett in 1970 [16] (see also Ref. [17] for an earlier proposal of a solid phase of interacting Bosons). After decades of inconclusive searches in helium systems [18], the first clear demonstrations of supersolidity were achieved in ultracold atomic gases, specifically in dipolar quantum gases [19–21], spin-orbit-

coupled Bose-Einstein condensates [22], and by coupling BEC in optical cavities [23]. Theoretical results for Rydberg-dressed atoms and soft core bosons suggested the possibility of realizing supersolid structures also in these systems [24, 25, 28–32]. Recent theory predicts the existence of binary dipolar supersolids, where two dipolar superfluids combine to form a periodically modulated state [26, 27].

The possibility of supersolid phases in a binary Bose mixture has recently been put forward in Ref. [33, 34], where a self-bound 2D supersolid stripe-phase in a weakly interacting binary BEC with spin-orbit coupling has been proposed, being stabilized by the Lee-Huang-Yang beyond-mean-field term. In Ref. [35], a single one-dimensional droplet made of a binary Bose mixture immersed into a background of the excess species and subject to periodic boundary conditions (as a model for a droplet confined in a toroidal trap), was found to display non-classical rotational inertia and thus the coexistence of rigid-body and superfluid character.

It has been suggested [36] that a droplet array resulting from the breakup, caused by the Rayleigh-Plateau instability, of a quantum liquid filament made of a K-Rb Bose mixture, and where atoms of one species are in excess with respect to the optimal equilibrium ratio, may display supersolid character.

The rich physics of quantum droplets and supersolids has primarily been investigated in single- and two-components dipolar gases and two-component Bose mixtures, whereas the possibility of observing these phenomena in three-component systems remains largely unexplored. In a recent theoretical work [37] cluster formation in three-component ultracold bosons has been investigated, in the form of Borromean cluster, where only the ternary

bosons can form a self-bound droplet while any binary subsystems cannot. A paper appeared later[38] where a new type of shell-shaped Bose-Einstein condensate with a self-bound character has been proposed, made of three-component ^{23}Na ^{39}K ^{41}K Bose mixture (species (1,2,3) in the following), where the mixtures (1,2) and (2,3) both form self-bound droplets. In the proposed structures an outer shell of liquid (1,2) envelops a spherical core made of the (2,3) liquid, and it was claimed to be stable without the need of any trapping potential. As shown in Ref.[39], however, it turns out that these structures are not actually the ground-states solutions to the system but rather metastable states corresponding to local energy minima. The lowest energy state is instead a "dimer" configuration where two quantum droplets (made of the (1,2) fluid and (2,3) fluid, respectively) are bound together by the shared component 2 [39].

Starting from this finding, I found that a simple protocol (easily implementable in real experiments) may result in the formation of a more complex structure where multiple dimers are bound together in a linear structure, which has supersolid character.

The system described here consists of linear chains of alternating quantum droplets (quantum "diatomic" linear chain), each composed of mixtures of components (1,2) and (2,3), where component (2) acts as a "glue" connecting adjacent droplets, and it is stable in vacuum, i.e. no trapping potential is required for its stabilization.

This structure displays supersolid properties, in the form of finite non-classical translational inertia. This configuration presents therefore a unique opportunity to study the interplay between quantum droplet formation, supersolidity, and the role of a mediating component in a reduced-dimensional setting.

The remainder of this paper is organized as follows: In Section II, the theoretical model and the numerical methods used for the calculations are presented. Section III describes results for the building block of the proposed supersolid, i.e. the quantum dimer. In Section IV the properties of the "diatomic" linear chain made by periodic repetitions of dimers along the chain axis, and its supersolid character are investigated, together with its vibrational properties. Finally, Section V contains a summary and outlook for future research directions.

II. METHOD

The system under study here is the same as in Ref.[38], i.e. a three-component ^{23}Na ^{39}K ^{41}K Bose mixture, at zero temperature and in the absence of three-body recombination effects. An inhomogeneous mixture made of the above species is described within the density functional theory (DFT) approach in the MF+LHY framework, where the total energy functional is given by (atomic units will be used hereafter)

$$E = \sum_{i=1}^3 \int d\mathbf{r} \frac{1}{2m_i} |\nabla\psi_i(\mathbf{r})|^2 + \frac{1}{2} \sum_{i,j=1}^3 g_{ij} \int d\mathbf{r} \rho_i(\mathbf{r})\rho_j(\mathbf{r}) + \int d\mathbf{r} \mathcal{E}_{LHY}(\rho_1(\mathbf{r}), \rho_2(\mathbf{r}), \rho_3(\mathbf{r})) \quad (1)$$

Here $\rho_i(\mathbf{r}) = |\psi_i(\mathbf{r})|^2$ represent the number density of each component ($i = 1$ for ^{23}Na , $i = 2$ for ^{39}K and $i = 3$ for ^{41}K). The coupling constants between species i and j are $g_{ij} = 2\pi a_{ij}/m_{ij}$, with scattering length a_{ij} and reduced mass $m_{ij} = m_i m_j / (m_i + m_j)$. The number densities ρ_i are normalized such that $\int_V \rho_i(\mathbf{r}) d\mathbf{r} = N_i$ ($i = 1, 2, 3$), where N_i are the total number of atoms in the i -th component.

Components 1 and 3 interact via strong repulsive potential and are therefore immiscible, while the binary mixtures (1,2) and (2,3) separately form self-bound binary droplets. As shown in Ref.[38], this is achieved with $(a_{11}, a_{22}, a_{33}, a_{12}, a_{13}) = (52, 30, 63, -50, 213)a_0$ (a_0 is the Bohr radius), while a_{23} (which is highly tunable via a Feshbach resonance) must have a negative, and sufficiently large, value. I will consider here the same two representative values used in Ref.[38], $a_{23} = -70a_0$ and $a_{23} = -200a_0$, although, due to the heavy compu-

tational cost, most of the calculations will be performed with $a_{23} = -200a_0$. The choice of this value is motivated by the fact that it gives stronger binding between droplets and therefore clearer signals in the computed spectra (as discussed in the following Sections).

The term accounting for quantum fluctuations is

$$\mathcal{E}_{LHY} = \int \frac{d^3\mathbf{k}}{2(2\pi)^3} \left[\sum_i (E_{i\mathbf{k}} - \epsilon_{i\mathbf{k}} - g_{ii}\rho_i) + \sum_{ij} \frac{2m_{ij}g_{ij}^2\rho_i\rho_j}{\mathbf{k}^2} \right] \quad (2)$$

with $\epsilon_{i\mathbf{k}} = k^2/2m_i$, and $E_{i\mathbf{k}}$ is the i -th Bogoliubov excitation energy [37]. The three dispersion relations $E_{i\mathbf{k}}$ ($i = 1, 2, 3$) are the roots of the following equation [37]

$$x^3 + bx^2 + cx + d = 0, \quad (3)$$

where

$$b = -\sum_i \omega_i^2, \quad (4)$$

$$c = \sum_{i<j} ((\omega_i \omega_j)^2 - 4g_{ij}^2 \rho_i \rho_j \epsilon_{ik} \epsilon_{jk}), \quad (5)$$

$$d = -(\omega_1 \omega_2 \omega_3)^2 - 16\epsilon_{1k} \epsilon_{2k} \epsilon_{3k} g_{12} g_{23} g_{13} \rho_1 \rho_2 \rho_3 + \sum_{i<j, l \neq (i,j)} 4\epsilon_{ik} \epsilon_{jk} \rho_i \rho_j g_{ij}^2 \omega_l^2. \quad (6)$$

Here $\omega_i = \sqrt{\epsilon_{ik}^2 + 2g_{ii}\rho_i\epsilon_{ik}}$ ($i = 1, 2, 3$) are the Bogoliubov spectra for the individual components [40].

Minimization of the action associated to Eq.(1) leads to the following Euler-Lagrange equations

$$i \frac{\partial \psi_i(\vec{r}, t)}{\partial t} = \left(-\frac{\nabla^2}{2m_i} + \sum_j g_{ij} \rho_j + \frac{\partial \mathcal{E}_{LHY}}{\partial \rho_i} \right) \psi_i(\vec{r}, t) \quad (7)$$

The numerical solutions of Eqs.(7) provide the real-time evolution of the system in three-dimensional space. When stationary states are sought the left hand side of Eq.(7) is replaced by $\mu_i \psi_i(\vec{r})$, where μ_i is the chemical potential of the i -th species. The evolution in imaginary time (via, e.g., steepest descent algorithm) allows to obtain stationary state solutions starting from suitable initial wavefunctions. The chemical potentials μ_i are determined iteratively so that the target values of N_i are achieved.

The wave functions $\{\psi_i\}$ are mapped on an equally spaced 3D Cartesian grid and the Laplacian operator in Eq.(7) is represented by a 13-point finite-difference stencil. The equations (7) are propagated in real time by using the Hamming's predictor-modifier-corrector method initiated by a fourth-order Runge-Kutta-Gill algorithm [42]. Periodic boundary conditions (PBC) are imposed along the three spatial directions. The mesh spacing and time step are chosen such that during the real time evolution excellent conservation of the total energy of the system is guaranteed.

III. THE "DIMER" CONFIGURATION

The self-bound, shell-shaped structure investigated in Ref.[38] is made of three-component ^{23}Na ^{39}K ^{41}K Bose mixture, where the mixtures (1,2) and (2,3) both form quantum droplets. In the structure proposed in Ref.[38] an outer shell of liquid (1,2) envelops a spherical core made of the (2,3) liquid, and it is claimed to be stable without the need of any trapping potential. However, this turns out to be a *metastable* state [39]: any perturbation would make these structures swiftly convert into the actual lowest energy state, characterized by a "dimer" configuration, where two self-bound droplets (made of the (1,2) fluid and (2,3) fluid, respectively) are kept in mutual contact by the shared component 2.

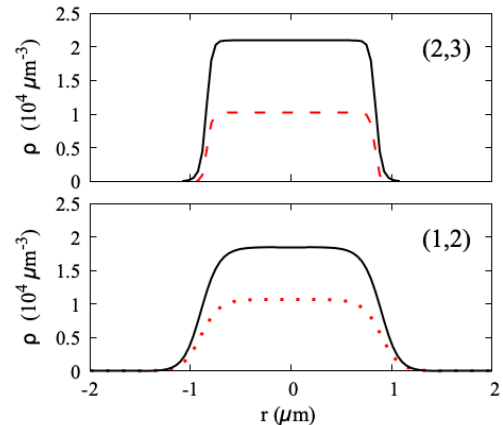


FIG. 1. Density profiles of the individual self-bound droplets made of liquid (2,3) (upper panel) and (1,2) (lower panel). Dotted line: species 1; solid line: species 2; dashed line: species 3.

In Fig.1 the equilibrium densities of two separate self-bound droplets are shown, for the case $a_{23} = -200 a_0$. The first (1,2) droplet is made of $N_1 = 3.5 \times 10^4$ and $N_2 = 5.9 \times 10^4$ atoms, while the second (2,3) droplet is made of $N_2 = 5.4 \times 10^4$ and $N_3 = 2.5 \times 10^4$ atoms. The total masses of each droplet, which will be relevant in the discussion of the dimer vibrational properties, are $M_{12} = N_1 m_1 + N_2 m_2 = 5.66 \times 10^9$ and $M_{23} = N_2 m_2 + N_3 m_3 = 5.71 \times 10^9$ (expressed in atomic units).

In the interior of each droplet, the equilibrium density ratio ρ_j/ρ_i is locked at the value $\sqrt{g_{ii}/g_{jj}}$ [5, 38], as expected from the theory of binary Bose mixtures.

In Fig.2 and Fig.3 is shown the "dimer" equilibrium structure resulting from the interaction between the two droplets, the binding being a consequence of sharing the component (2) between the two droplets. Notice that, while the number of atoms N_1 and N_3 can be fixed independently, the number of atoms N_2 should be taken close to the ideal number $N_2 = N_2^{(1)} + N_2^{(2)}$, where $N_2^{(1)}$ and $N_2^{(2)}$ are such to satisfy the equilibrium ratio in the interior of the droplets, $N_1/N_2^{(1)} \sim \sqrt{g_{22}/g_{11}}$ and $N_2^{(2)}/N_3 \sim \sqrt{g_{33}/g_{22}}$.

For comparison, the stable dimer configuration is shown in Fig.4 for a lower value $a_{23} = -70 a_0$. It appears that due to the weaker coupling between species

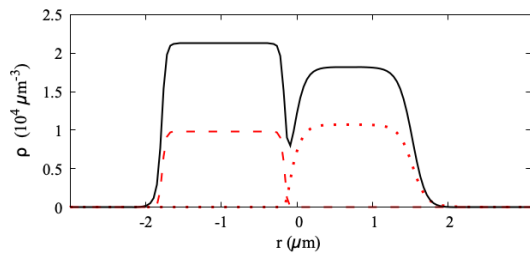


FIG. 2. Dimer density profile along the line passing through its axis, for the case $a_{23} = -200 a_0$. Dotted line: species 1; solid line: species 2; dashed line: species 3.

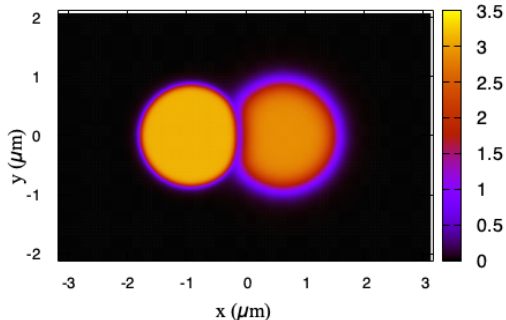


FIG. 3. Total density map corresponding to the dimer structure shown in Fig. 2. The droplet (2,3) is on the left, the droplet (1,2) on the right. The density units are the same as in Fig. 2)

(2,3), the contact area between the two droplets is reduced with respect to the case $a_{23} = -200 a_0$. The resulting lower binding between the two droplets will show up, as discussed in the following, in a lower frequency of the dimer bond-length oscillations.

Below, I briefly discuss the vibrational properties of the dimer structure shown in Figs. 2-3.

It is useful in this regard to preliminary study the intrinsic oscillations of the individual droplet components (see Fig. 1). In particular, the frequencies $\omega_{l,n}$ of the lowest angular momentum modes will be computed, i.e. $l = 0, n = 0$ (monopole "breathing" mode) and $l = 2, n = 0$ (quadrupole mode). The frequency of the $l = 1, n = 0$ (dipole mode) is zero, corresponding to a rigid translation of the droplet as a whole.

To extract the frequency of such modes, I applied to the ground-state wavefunctions ψ_i of each droplet (providing the equilibrium configurations shown in Fig. 1) a perturbation such that the initial states for the dynamics are $\psi_i^{ini} = e^{i\epsilon F} \psi_i$ where $F = r^2$ for the monopole mode, $F = (3z^2 - r^2)$ for the quadrupole mode, and ϵ is a small number. The system is then allowed to evolve in real-time starting from ψ_i^{ini} . The average value of the moments during the dynamics is recorded, $\langle F(t) \rangle = \langle \psi_i(t) | F | \psi_i(t) \rangle$, and finally it is Fourier transformed into the frequency domain, $\tilde{F}(\omega) = \int \langle F(t) \rangle e^{i\omega t} dt$.

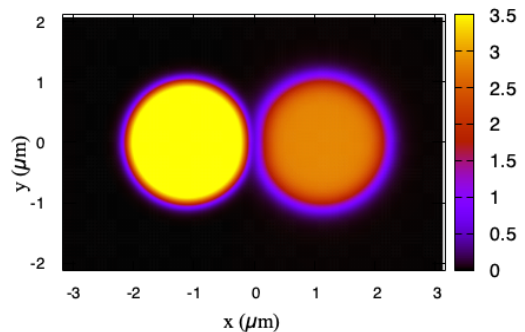


FIG. 4. Total density map corresponding to the dimer structure with $a_{23} = -70 a_0$. The droplet (2,3) is on the left, the droplet (1,2) on the right. The density units are the same as in Fig. 2.

The peaks in $\tilde{F}(\omega)$ allow to extract the sought frequencies. I found $\omega_{quad}^{(1,2)} = 1198$ Hz, while $\omega_{quad}^{(2,3)} = 2045$ Hz. The monopole modes have much higher frequencies, $\omega_{mono}^{(1,2)} = 4850$ Hz and $\omega_{mono}^{(2,3)} = 17700$ Hz.

Interestingly, the dimers shown in Fig. 3 and Fig. 4 display simple vibrational patterns similar to a classical spring-mass model, where the two droplets forming the dimer oscillate back and forth around their equilibrium positions. In order to show this, an initial small velocity boost is applied to the ground-state wavefunctions ψ_i , $\psi_i^{ini} = \psi_i e^{\pm i k x}$ where $k = m_i v$. The initial velocity is $v = 0.5 \times 10^{-10} a_0 E_h / \hbar$. The sign is chosen so that the two droplets (1,2) and (2,3) are pushed towards one another at $t = 0$. The system is then left to evolve in real time, by solving the time-dependent equations (7). The time dependence of the bond length $d(t)$ (defined as $d = \langle x \rangle_{12} - \langle x \rangle_{23}$, in terms of the center-of-mass of the two droplets), is calculated and its Fourier transform $\tilde{f}(\omega) = \int e^{i\omega t} d(t) dt$ provides the dimer vibrational spectrum. This is shown with solid line in Fig. 5. The peak position in Fig. 5 gives the frequency $\Omega_d / (2\pi) = 576$ Hz for the dimer bond-length oscillation. Similar calculation, done for the case $a_{23} = -70 a_0$, gives a lower frequency for the dimer oscillation, $\Omega_d / (2\pi) = 305$ Hz. The associated vibrational spectrum is shown with a dotted line in Fig. 5. Additional features appear in both spectra at lower frequencies which might arise from mode-mixing between the dimer bond-stretching motion and low-energy superfluid (Goldstone) excitations of the superfluid background provided by the shared component 2. Evidence supporting this interpretation will be given when discussing the vibrational spectra of the diatomic chain in Section IV.

Due to the superfluid nature of the two droplets in the dimer structure, the hydrodynamic modes describing internal oscillations (multipole modes) associated with the superfluid nature of the system are expected to be excited as well during the dimer dynamics. To check for their

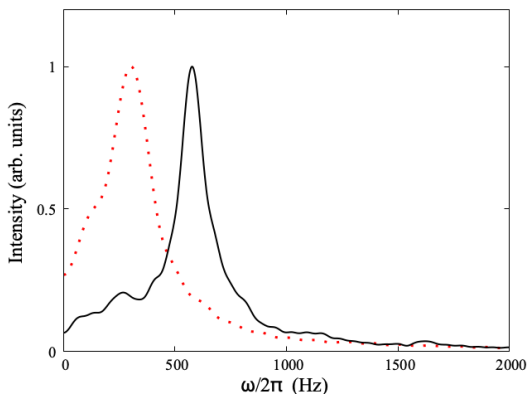


FIG. 5. Spectrum for the dimer oscillations. Solid line: $a_{23} = -200 a_0$, dotted line: $a_{23} = -70 a_0$.

presence, the values of the monopole and quadrupole moments $\langle F(t) \rangle = \langle \psi_i(t) | F | \psi_i(t) \rangle$ are calculated during the dimer oscillations and later Fourier analyzed, as described in the case of the isolated droplets.

In particular, the monopole and quadrupole spectra of the species 1 and the species 3 are computed separately. By assuming that during the dynamics the species 2 follows the local changes in densities of the other two species in each droplets, so that the density ratios ρ_1/ρ_2 and ρ_2/ρ_3 remains close to the equilibrium value for the individual droplets, then the computed moments should reflect the intrinsic dynamics of the two droplets that make up the whole dimer. Notice that in this way only excitations where the two species in each droplet move in-phase with respect to each other are considered, that cause large center-of-mass displacements/bond-length oscillations with little relative phase change, and thus emphasizes the mass-spring (bond-stretching) mode. Excitations characterized by out-of-phase displacements are therefore not included in the present analysis, but will be considered in the analysis of the vibrations of the diatomic chain in Section IV.

The Fourier transform in the time domain $\tilde{f}(\omega)$ are shown in the two panels of Fig.6 for the monopole and quadrupole mode, respectively. The two curves in each panel show the computed moment (monopole or quadrupole) in the species 1 (solid line) and the species 3 (dotted line). Besides the main peak at 576 Hz coming from the droplet-droplet oscillations discussed in Fig.5, peaks close to the monopole and quadrupole frequencies of the individual droplets are clearly visible.

Notice that additional small features are present in the Fourier spectrum, especially between 1000 and 2000 Hz, revealing a richer excitation spectrum for the dimer case, where monopole and quadrupole modes are coupled. Finite-size, nonlinearity effects and the intertwined nature of the three species complicate the interpretation of the vibrational spectra, making a precise assignment

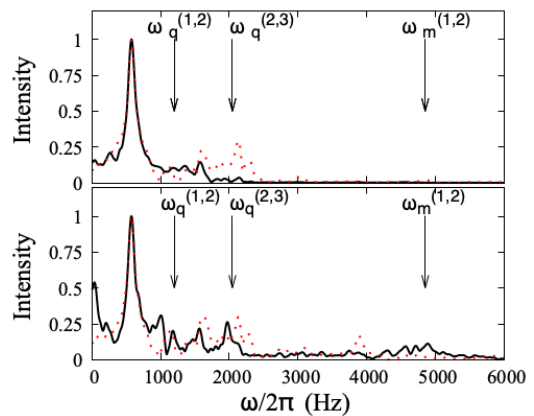


FIG. 6. Lower panel: spectrum for the monopole oscillations, for the case $a_{23} = -200 a_0$. Upper panel: spectrum for the quadrupole oscillations

of such modes quite difficult.

Similar coexistence between "mass-spring" modes and superfluid (hydrodynamical) modes is not new: classical-linear-chain behavior for droplet systems has been observed in the case of linear arrays of dipolar droplets. The vibrational patterns of isolated-droplet crystals that time-evolve after a small initial kick closely follow the properties of a classical linear chain, where droplets play the role of atom in classical monoatomic linear chain [43].

IV. THE SUPERSOLID "DIATOMIC" LINEAR CHAIN

The dimer configuration described in the previous Section, and its properties, suggest the possibility of engineering more complex structures arranging multiple dimers. The simplest possibility, which is studied here, is a linear chain made of a sequence of droplets $\dots(1,2)-(2,3)-(1,2)-(2,3)-(1,2)-(2,3)\dots$. I will describe here a simple method, used in the present simulations, which could be easily translated into an experimental protocol to practically realize such structure. In the following, the x -axis will be the axis of the linear chain of droplets. Due to the high computational cost of the simulations, I will consider in the following only the case with $a_{23} = -200 a_0$, although similar phenomenology is expected for the case with $a_{23} = -70 a_0$ (or any intermediate value for that matter).

A *uniform* mixture of the three types of atoms is considered, subject to an external waveguide potential (the same for all three species) of the form $(1/2)m_i\omega_r^2 r^2$ ($i = 1, 2, 3$) where $r^2 = y^2 + z^2$ is the radial coordinate perpendicular to the axis of the waveguide, and $\omega_r = (2\pi) \times 300$ Hz. Due to the use of Periodic Boundary Conditions in the present calculations, the system effectively forms an infinitely extended "tubular" geometry

(or, equivalently, a ring geometry if curvature effects can be neglected). Let L_x be the length of the simulation cell along the tube axis.

An additional weak optical potential is also applied along the x -axis, which has the purpose of modulating, along the tube axis, the uniform mixture localized within the waveguide, and trigger the separation into (1,2) and (2,3) droplets. This potential has the form $V(x) = V_0 \sin^2(kx)$, where $k = \pi/a_L$ and a_L is the "lattice constant", i.e. the length of the basic unit cell which will eventually contain a single dimer and whose periodic repetition will provide the chain sequence ... (1,2)-(2,3)-(1,2)-(2,3)-(1,2)-(2,3)... I took $V_0 = 10^{-13} E_h$ as a representative value for a weak modulation, although other choices for this parameter will work as well.

The atom numbers N_1 , N_2 and N_3 are chosen so that an integer number of dimers like the one shown in Fig.3 can be accommodated in a supercell of given length L_x along the x -direction. Here I took $N_1 = 1.4 \times 10^5$, $N_2 = 4.5 \times 10^5$ and $N_3 = 10^5$ atoms, corresponding to a total of four dimers, i.e. $L_x = 4a_L$. A precise choice for the number of atoms or for the simulation cell length L_x is however not critical for the realization of the final chain structure nor for its supersolid character: even for imbalanced mixtures, the excess population of one species with respect to the equilibrium value of an isolated droplet will be expelled from it and contribute to a uniform background, where the chain modulated structure is immersed. In particular, this background is expected to further contribute to the chain supersolid fraction (see the following), and therefore to its supersolid properties. Similarly, a different choice for L_x will result in a compressed/elongated chain, without jeopardizing the supersolid formation.

During the minimization in imaginary time, the initial homogeneous mixture under the effect of the external potentials spontaneously separates into (1,2) and (2,3) mixtures, which form a regular sequence of droplets of alternating type. The structure found is an infinitely extended linear chain where the primitive cell of length a_L contains a "basis" made of the (1,2)-(2,3) dimer. The external potential (both the radial and the longitudinal ones) are then removed, and the imaginary-time evolution is continued until convergence.

We note that if the structure minimization is performed in the absence of the modulating potential (but still maintaining the radial confining potential), as a result a highly "defective" structure is eventually obtained, where the system indeed spontaneously undergo fragmentation in two type of droplets, but with different sizes of the same type of droplets, and large distortions of the droplet themselves.

The resulting structure is an equilibrium configuration in vacuum, meaning that no confining potential is required to stabilize the final chain structure. In practice, however, a radial confinement might be kept active in

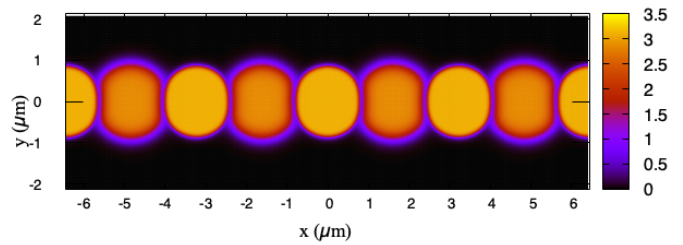


FIG. 7. Total density maps corresponding to the diatomic chain structure with $a_{23} = -200 a_0$. The density units are the same as in Fig.2.

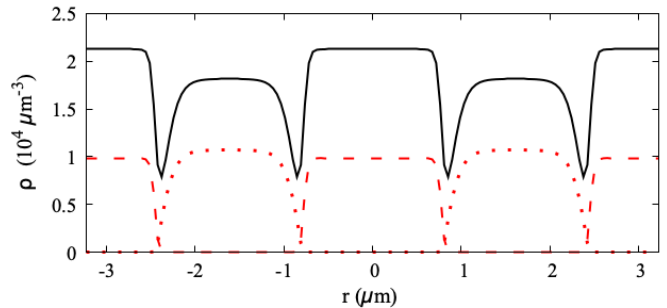


FIG. 8. Density profiles along the axis of the chain structure of Fig.7. For clarity, only one half of the chain in Fig.7 is shown here. Dotted line: species 1; solid line: species 2; dashed line: species 3.

actual experimental realizations to avoid possible instabilities of the chain due to axial undulations which may destabilize it.

The final step is to optimize the lattice constant, i.e. the parameter a_L is varied (at fixed number of atoms) until the energy is minimized. I found in this way for the equilibrium lattice constant the value $a_L = 3.23 \mu m$. The final ground-state configuration is shown in Fig.7 and Fig.8.

The bond length (defined as the distance between the center-of-mass of two adjacent droplets) turns out to be $d = a_L/2 = 1.61 \mu m$, which is smaller by $\sim 5\%$ than the bond-length in the isolated dimer in Fig.3 ($d = 1.69 \mu m$), indicating an increased binding between adjacent droplets when the chain is formed out of individual dimers. In terms of the mass-and-spring model, this implies that the force constant \tilde{K}' between adjacent droplets in the chain is larger than the one characterizing the oscillations of the isolated dimer, as shown in the following.

A similar protocol to the one described previously to

nucleate a diatomic linear chain allows to realize a super-solid diatomic chain in the case $a_{23} = -70 a_0$. The resulting structure (not shown) has a larger lattice constant, reflecting the lower binding between droplets of different types, and it is characterized by a smaller overlap between adjacent droplets compared with the one obtained with $a_{23} = -200 a_0$, similarly to the case of the dimer structures.

We must note at this point that during the droplet formation process in any experimental attempt to create such structure, transient local excitations (surface modes of nascent droplets, breathing/vibrational modes, relative-phase distortions between droplets), coming from the sudden local density rearrangement, are expected to be created and should be subsequently damped by redistribution of kinetic energy in the system. The imaginary-time minimization used here to create the droplet chain suppresses most of these transients. The effect of excitations created during droplet formation could be revealed only by a full real-time dynamics simulation of the whole process, which however I did not attempt here.

The systems discussed here shows both density modulations and phase coherence (guaranteed by the common background of the species (2)), which are the prerequisites for supersolidity. I have therefore looked for the signature of the free flow of the superfluid fraction of system through its periodically modulated structure, namely a finite non-classical translational inertia.

Following Refs.[44, 45], the superfluid fraction f_s can be defined as the fraction of particles that remain at rest in the comoving frame with a constant velocity v_x . This is found by solving for stationary states the equation (7) in the reference frame moving with constant velocity v_x , i.e.

$$i \frac{\partial}{\partial t} \psi_i(\mathbf{r}) = (H_0 + i v_x \frac{\partial}{\partial x}) \psi_i(\mathbf{r}) \quad (8)$$

(H_0 being the Hamiltonian operator within round brackets in Eq.(7)) and then computing the superfluid fraction

$$f_s = 1 - \lim_{v_x \rightarrow 0} \frac{\langle (P_{x,1} + P_{x,2} + P_{x,3}) \rangle}{(N_1 m_1 + N_2 m_2 + N_3 m_3) v_x}, \quad (9)$$

where $\langle P_{x,j} \rangle = -i \int (\psi_j^* \partial \psi_j / \partial x) d\vec{r}$ is the expectation value of the momentum of the j -th species and $(N_1 m_1 + N_2 m_2 + N_3 m_3) v_x$ is the total momentum of the system as if all droplets were moving as rigid bodies. A non-zero value for f_s reveals global phase coherence in a periodic system like the one studied here, and therefore supersolid character.

I found in this way, for the chain structure shown in Fig.7, the value $f_s = 0.71$. Not surprisingly, almost all the contribution to the superfluid fraction comes from the shared component 2, which forms a background with large overlap in the interstitial region between one droplet and the next, as it appears from Fig.8.

Alternatively, one could estimate an upper bound of the (component-resolved) superfluid fraction using Leggett's formula [16] separately for each species:

$$f_s^{(i)} = (\langle n_i \rangle \langle n_i^{-1} \rangle)^{-1} \quad (10)$$

where

$$\langle n_i \rangle = (1/L_x) \int_0^{L_x} dx \langle \rho_i \rangle \quad (11)$$

$$\langle n_i^{-1} \rangle = (1/L_x) \int_0^{L_x} dx \langle \rho_i \rangle^{-1} \quad (12)$$

and $\langle \rho_i \rangle$ is the number density of the ground-state configuration for the i -th species averaged over the transverse y-z directions. Here L_x is the length of the simulation cell along the chain axis. The calculated fractions are: $f_s^{(1)} = 0.05$, $f_s^{(2)} = 0.82$, $f_s^{(3)} \sim 0$, confirming the main role played by the shared component 2. The system therefore behaves as a composite supersolid where the supersolid mass transport is dominated by a single delocalized component (species 2) that connects droplets.

I now discuss some vibrational properties of the supersolid chain structure described above.

First notice that a spring-and-mass model for the vibrations of an isolated dimer where the two atoms move back and forth with a periodic motion of frequency Ω_d , as discussed in the previous Section, gives $\Omega_d = \sqrt{\tilde{K}/\mu}$, where $\mu = M_{12} M_{23} / (M_{12} + M_{23})$ is the reduced mass of the two droplets and \tilde{K} is the force constant. In the present case we have $M_{12} \sim M_{23} \equiv M$, and therefore $\Omega_d = \sqrt{2\tilde{K}/M}$. A numerical estimate for \tilde{K} can be obtained by using the computed value of Ω_d from Fig.5.

The lattice of the supersolids structure investigated here can be described by a periodically repeated primitive cell containing a "two-atom" basis (the (1,2) and (2,3) droplets), and further understanding may be obtained by analogy with the dynamics of non-superfluid crystals, i.e. a classical diatomic linear chain made of particles with alternating masses M_{12} and M_{23} , connected by a spring with constant \tilde{K}' , where $\tilde{K}' > \tilde{K}$ (see the discussion following the presentation of Fig.7 and Fig.8).

In ordinary crystal lattices with two atoms per primitive cell (of length a_L), the phonon branch of a monatomic linear crystal is replaced by a gapped spectrum, with the lower acoustic (upper optical) branch being characterized by in-phase (out-of-phase) motions between nearest neighbors. Fig.9 shows schematically the displacement patterns of atoms in a diatomic linear chain at two relevant points in the 1st Brillouin Zone (BZ) along the chain axis, i.e. the zone-center $k = 0$ and the point at the zone boundary, $k = \pi/a_L$. The longitudinal acoustic mode at $k = 0$ (not shown in the Figure) is just a rigid

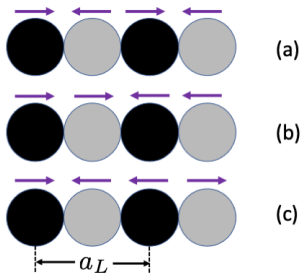


FIG. 9. Displacement patterns for the different longitudinal modes of a diatomic linear chain: (a) $k = 0$ optical oscillation (with frequency $\omega_O(k = 0)$); (b) $k = \frac{\pi}{a_L}$ acoustic oscillation (with frequency $\omega_A(k = \pi/a_L)$); (c) $k = \frac{\pi}{a_L}$ optical oscillation (with frequency $\omega_O(k = \pi/a_L)$). The two vertical dotted lines shows the unit cell of length a_L .

translation of the chain as a whole along the x-axis, and as such has zero frequency.

The frequencies of the longitudinal modes in classical diatomic linear chain, whose patterns are shown in Fig.9, are $\omega_O(k = \pi/a_L, \text{optical}) = \sqrt{2\tilde{K}/M} = \Omega_d$, $\omega_A(k = \pi/a_L, \text{acoustic}) = \sqrt{2\tilde{K}/M} = \Omega_d$, $\omega_O(k = 0, \text{optical}) = \sqrt{2\tilde{K}/\mu} = \sqrt{2}\Omega_d$. The two zone-boundary modes are degenerate because the masses M_{12} and M_{23} of the two droplets are almost equal, as already discussed.

In general, for linear supersolids a Goldstone branch of superfluid phonons associated with the condensate order parameter is expected to appear, besides the crystal phonon branch characteristic of a regular solid [46]. The periodic modulation of the density reduces the superfluid fraction [16] and the lower phonon branch (superfluid mode) has a second-sound character, while the upper branch (lattice phonon mode) consists of first-sound-like modes [47].

In fact, recent experimental observation [49] in dipolar quantum gas showed that when the system enters supersolid state, low energy compressional modes (which emerge naturally from the hydrodynamics equations of superfluidity and must therefore be associated with the finite superfluid fraction) bifurcates into two distinct excitations (similarly with the appearance of the gapless Goldstone excitations expected for homogeneous supersolid): the higher-frequency mode is related to the lattice deformations (relative displacements of the droplets making the chain), while the lower mode is instead related to compressional excitations of the superfluid components.

In order to excite the proper (longitudinal) oscillation mode in the supersolid chain described here I proceeded as follows: a small perturbation in the form of an axial density modulation along the supersolid axis is added to the equilibrium density at $t=0$:

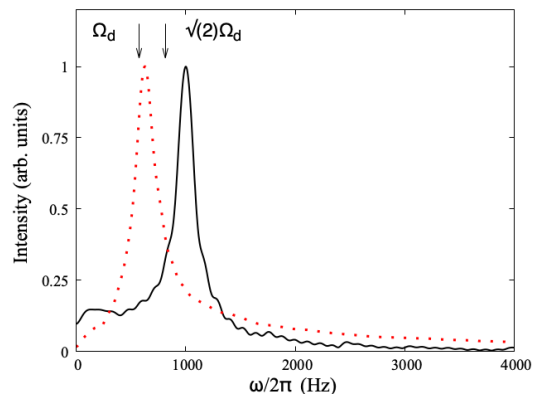


FIG. 10. Spectrum at $k = 0$ (solid line) and $k = \pi/a_L$ (dotted line). The vertical arrows indicate the positions expected for the classical diatomic chain modes.

$$\rho(\vec{r}) = \rho_0(\vec{r})[1 + \epsilon \cos(kx)] \quad (13)$$

with wave-vector k . Here $\rho_0(\vec{r})$ be the total ground-state density and ϵ is a small number. In order to reduce the computational cost calculations have been done for a linear chain which has a length along the x-axis which is one half of that illustrated in Fig.7, i.e. the basic cell for real-time dynamics is composed of two unit cells, each of length a_L containing two droplets (1,2) and (2,3). I considered two values for k , i.e. $k = 0$ (center of the 1st Brillouin zone along the chain axis), and $k = \pi/a_L$ (surface of the 1st Brillouin zone). The amplitude ϵ of the perturbation must be small: here I took $\epsilon = 0.025$. The system is thus left to evolve in real time. The density $\rho(\vec{r}, t)$ is computed at regular time intervals, and from the computed values the projection of the density onto the k -mode is calculated:

$$\rho(k, t) = \int_0^{L_x} dx e^{-ikx} \int dy \int dz \rho(x, y, z, t) \quad (14)$$

Finally, $\rho(k, t)$ is Fourier transformed into the frequency domain:

$$\rho(k, \omega) = \int dt \rho(k, t) e^{i\omega t} \quad (15)$$

to provide the mode frequencies as peaks in $\rho(k, \omega)$ (a similar method is used in Ref.[48] to probe one-dimensional supersolid states, but where a periodic optical potential is applied to excite the supersolid and determine its density excitation frequencies).

The above approach is feasible for any finite k -value whose wavelength $2\pi/k$ fits the cell length along the x-direction. In order to compute the optical modes at $k = 0$ another method is therefore required. I used here a simple strategy where a kick to the droplets composing the

chain is applied to excite the desired displacement pattern associated with the mode under study. An initial small velocity boost is applied to the ground-state wavefunctions ψ_i , $\psi_i^{ini} = \psi_i e^{\pm ikx}$ where $k = m_i v$. The initial velocity is $v = 0.5 \times 10^{-10} a_0 E_h/\hbar$. The sign is chosen so that the droplets (1,2) and (2,3) initial displacements match the pattern characterizing the optical mode at $k = 0$ (case (a) in Fig.9). The system is thus left to evolve in real time and the droplets relative displacements are Fourier analyzed in order to find the associated frequencies.

The results are shown in Fig.10 for both cases, $k = \pi/a_L$ and $k = 0$. Two main peaks are clearly visible: the lower frequency one ($k = \pi/a_L$) is associated with the (degenerate) acoustic and optical modes at the BZ boundary (cases (b) and (c) in Fig.9), while the higher frequency mode ($k = 0$) is associated with the zone-center optical mode (case (a) in Fig.9). Both frequencies are higher than those expected using the force constant estimated from the isolated dimer vibrations (shown by vertical arrows in the Figure). This is expected since the force constant for the chain is larger than the one for the dimer due to the increased binding in the chain with respect to the dimer case, as discussed before. We finally mention that dispersion relations showing similarities with a linear diatomic crystal has been found recently [50] in binary dipolar supersolid.

The dynamics described previously restricts the analysis to in-phase motion of the components in each droplet, and therefore emphasizes the mass-spring (bond-stretching) mode discussed above. To check whether low-energy, out-of-phase (odd-parity) modes - such as Josephson or Goldstone type phase oscillations that are connected to global phase coherence in supersolids [51, 52] - are present, we performed additional real-time simulations where an initial small relative phase difference with $k = \pi/a_L$ (i.e. at the boundaries of the first BZ) was imprinted on the shared ^{39}K component (which is the relevant one for the superfluid character throughout the system). In particular, the initial wavefunction $\psi_2(\vec{r})$ is obtained from the ground-state one $\psi_2^{(0)}(\vec{r})$ as

$$\psi_2(\vec{r}, t = 0) = \psi_2^{(0)}(\vec{r}) e^{i\Delta\phi \cos(\pi x/a_L)} \quad (16)$$

where the amplitude $\Delta\phi$ is chosen small (~ 0.02) to remain in the linear regime. Then, during the real time evolution, I computed

$$\psi_2(k, t) = \int_0^{L_x} dx e^{-ikx} \int dy \int dz \psi_2(x, y, z, t) \quad (17)$$

Finally, $\psi_2(k, t)$ is Fourier transformed into the frequency domain:

$$\psi_2(k, \omega) = \int dt \psi_2(k, t) e^{i\omega t} \quad (18)$$

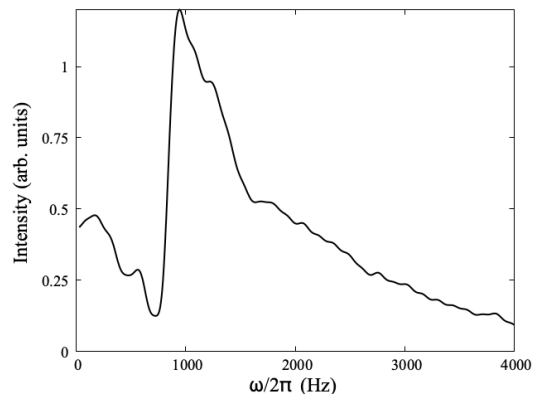


FIG. 11. Spectral function $|\psi_2(k, \omega)|$ at $k = \pi/a_L$.

to provide the mode frequencies as peaks in $|\psi_2(k, \omega)|$. The resulting spectrum is shown in Fig.11, where $|\psi_2(k = \pi/a_L, \omega)|^2$ is plotted, showing low-frequency branches (below 500 Hz) which should be associated with out-of-phase oscillations of the condensate phase (Goldstone/Josephson character) distinct from the higher-frequency lattice phonon branches (a more detailed analysis of the shown spectrum is however difficult, for the same reasons described when commenting the spectra in Fig.6). These results provide independent dynamical evidence of global phase coherence and further support the supersolid nature of the diatomic chain structure.

V. CONCLUSIONS AND OUTLOOK

In this work, I have theoretically investigated the formation and properties of a supersolid structure in a three-component ultracold Bose gas mixture composed of ^{23}Na , ^{39}K , and ^{41}K atoms, in the form of an extended linear chain structure, stable in vacuum. This structure is made by periodic repetition of the basic building block represented by a "dimer" unit consisting of two weakly bound quantum droplets, made of (1,2) and (2,3) species.

The dynamics of an isolated dimer shows the coexistence of stretching vibrations as in mass-and-spring model, where the dimer bond length oscillates harmonically in time, and hydrodynamical modes associated with the superfluid nature of the system.

A protocol is presented, which could be implemented in experimental realization, to create a linear chain structure starting from a homogeneous three-component mixture subject to a suitable external potential, which results in the spontaneous formation of an alternating sequence of (^{23}Na , ^{39}K) and (^{39}K , ^{41}K) droplets.

This "diatomic linear chain" structure exhibits both periodic density modulations arising from the droplet ordering and global phase coherence, facilitated by the shared ^{39}K component, therefore satisfying the criteria for supersolidity. A relevant superfluid fraction is in-

deed found by computing the non-classical translational inertia of the system. The excitation spectrum of the supersolid chain is investigated by probing its response to density perturbations. I identified longitudinal vibrational modes corresponding to crystal lattice oscillations like acoustic and optical phonon modes expected from a classical diatomic chain, coexisting with low-frequency out-of-phase oscillation of the condensate phase.

The supersolid phase studied here is qualitatively distinct from previously studied realizations, the broken translational symmetry and global phase coherence arising from a mediated droplet binding mechanism rather than from long-range forces or momentum-space interference. In contrast to dipolar systems (where long-range dipole-dipole interactions and roton softening set the periodicity of the supersolid) this provides several new handles (interspecies scattering lengths, relative populations and mass imbalance) to tune the lattice spacing, the coupling strength between droplets, the relative sizes of the two types of droplets and the resulting superfluid fraction, potentially accessing regimes that are difficult to reach in dipolar or spin-orbit platforms. Therefore this supersolid chain represents a novel tunable quantum phase in multi-component systems, with potential for experimental realizations using state-of-the-art ultracold atom setups. Although the experimental implementation of a three-species setup is likely more demanding than two-component or single-species realizations, the extra experimental complexity might be compensated by the increased tunability and by the qualitatively new phenomena this platform can explore.

Future research directions could include exploring the stability and dynamics of the supersolid chain under various external perturbations, including the effect of transverse excitation modes, as well as investigating the effects of dimensionality and geometrical constraints on the formation and properties of such structure. Another interesting line in future research would be the study of vortices hosted by crystal configurations of the three-component supersolid, which is the most direct evidence of superfluidity in a supersolid structure response to rotation. For instance, a 2-D periodic array of (1,2) and (2,3) droplets subject to rotation around the axis perpendicular to the plane of the 2D "crystal", would be the ideal playground to study the formation and stability of quantized vortices [53].

I wish to thank G. Mistura and L. Salasnich for useful conversations. This work is supported by the Italian MIUR under the PRIN2022 Project No. 20227JNCWW.

[1] I. Bloch, J. Dalibard, and W. Zwerger, *Many-body physics with ultracold gases*, Rev. Mod. Phys. **80**, 885 (2008).

- [2] C. Chin, R. Grimm, P. Julienne, and E. Tiesinga, *Feshbach resonances in ultracold gases*, Rev. Mod. Phys. **82**, 1225 (2010).
- [3] C. Baroni, G. Lamporesi and M. Zaccanti, *Quantum mixtures of ultracold gases of neutral atoms*. Nature Reviews Physics **6**, 736–752 (2024).
- [4] L. Chomaz, I. Ferrier-Barbut, F. Ferlaino, B. Laburthe-Tolra, B.L. Lev and T. Pfau, *Dipolar physics: a review of experiments with magnetic quantum gases*, Reports on Progress in Physics **86**, 026401 (2023).
- [5] D. S. Petrov, *Quantum Mechanical Stabilization of a Collapsing Bose-Bose Mixture*, Phys. Rev. Lett. **115**, 155302 (2015).
- [6] I. Ferrier-Barbut, H. Kadau, M. Schmitt, M. Wenzel and T. Pfau, *Observation of Quantum Droplets in a Strongly Dipolar Bose Gas*, Phys. Rev. Lett. **116**, 215301 (2016).
- [7] H. Kadau, M. Schmitt, M. Wenzel, C. Wink, T. Maier, I. Ferrier-Barbut and T. Pfau, *Observing the Rosensweig instability of a quantum ferrofluid*, Nature **530**, 194 (2016).
- [8] M. Schmitt, M. Wenzel, F. Böttcher, I. Ferrier-Barbut and T. Pfau, *Self-bound droplets of a dilute magnetic quantum liquid*, Nature **539**, 259-262 (2016).
- [9] L. Chomaz, S. Baier, D. Petter, M.J. Mark, F. Wächtler, L. Santos and F. Ferlaino, *Quantum-Fluctuation-Driven Crossover from a Dilute Bose-Einstein Condensate to a Macrodroplet in a Dipolar Quantum Fluid*, Phys. Rev. X, **6**, 041039 (2016).
- [10] C.R. Cabrera, L. Tanzi, J. Sanz, B. Naylor, P. Thomas, P. Cheiney and L. Tarruell, *Quantum liquid droplets in a mixture of Bose-Einstein condensates*, Science, **359**, 301-304 (2018).
- [11] G. Semeghini, G. Ferioli, L. Masi, C. Mazzinghi, L. Wolswijk, F. Minardi, M. Modugno, G. Modugno, M. Inguscio and M. Fattori, *Self-Bound Quantum Droplets of Atomic Mixtures in Free Space*, Phys. Rev. Lett. **120**, 235301 (2018).
- [12] C. D’Errico, A. Burchianti, M. Prevedelli, L. Salasnich, F. Ancilotto, M. Modugno, F. Minardi, and C. Fort, *Observation of quantum droplets in a heteronuclear bosonic mixture*, Phys. Rev. Res. **1**, 033155 (2019).
- [13] Z. Guo, F. Jia, L. Li, Y. Ma, J.M. Hutson, X. Cui and D. Wang, *Lee-Huang-Yang effects in the ultracold mixture of ^{23}Na and ^{87}Rb with attractive interspecies interactions*, Phys. Rev. Res. **3**, 033247 (2021).
- [14] T.D. Lee, K. Huang, and C.N. Yang, *Eigenvalues and Eigenfunctions of a Bose System of Hard Spheres and Its Low-Temperature Properties*, Phys. Rev. **106**, 1135 (1957).
- [15] A.F. Andreev and I.M. Lifshitz, *Supersolidity of glasses*, Sov. Phys. JETP **29**, 1107 (1969).
- [16] A.J. Leggett, *Can a Solid Be "Superfluid"?*, Phys. Rev. Lett. **25**, 1543 (1970).
- [17] E.P. Gross, *Unified Theory of Interacting Bosons*, Phys. Rev. **106**, 161 (1957).
- [18] M.H.W. Chan, R.B. Hallock, and L. Reatto, *Overview on Solid ^4He and the Issue of Supersolidity*, J. Low Temp. Phys. **172**, 317 (2013).
- [19] L. Tanzi, E. Lucioni, F. Fama, J. Catani, A. Fioretti, C. Gabbanini, R.N. Bisset, L. Santos and G. Modugno, *Observation of a Dipolar Quantum Gas with Metastable Supersolid Properties*, Phys. Rev. Lett. **122**, 130405 (2019).
- [20] F. Böttcher, J-N. Schmidt, M. Wenzel, J. Hertkorn, M. Guo, T. Langen and T. Pfau, *Transient Supersolid Prop-*

- erties in an Array of Dipolar Quantum Droplets*, Phys. Rev. X **9**, 011051 (2019).
- [21] L. Chomaz, D. Petter, P. Ilzhofer, G. Natale, A. Trautmann, C. Politi, G. Durastante, R.M.W. van Bijnen, A. Patscheider, M. Sohmen, M.J. Mark and F. Ferlaino, *Long-lived and transient supersolid behaviors in dipolar quantum gases*, Phys. Rev. X **9**, 021012 (2019).
- [22] J.-R. Li, L. Lee, W. Huang, S. Burchesky, B. Shteynas, T.C. Furkan, A.O. Jamison and W. Ketterle, *A stripe phase with supersolid properties in spin-orbit-coupled Bose-Einstein condensates*, Nature **543**, 91 (2017).
- [23] J. Leonard, A. Morales, P. Zupancic, T. Esslinger and T. Donner, *Supersolid formation in a quantum gas breaking a continuous translational symmetry*, Nature **543**, 87 (2017).
- [24] L. Homeier, S. Hollerith, S. Geier, N-C. Chiu, A. Browaeys and L. Pollet, *Supersolidity in Rydberg tweezer arrays*, Phys. Rev. A **111**, L011305 (2025).
- [25] F. Cinti, P. Jain, M. Boninsegni, A. Micheli, P. Zoller and G. Pupillo, *Supersolid Droplet Crystal in a Dipole-Blockaded Gas*, Phys. Rev. Lett. **105**, 135301 (2010).
- [26] T. Bland, E. Poli, L.A. Pena Ardila, L. Santos, F. Ferlaino and R.N. Bisset, *Alternating-domain supersolids in binary dipolar condensates*, Phys. Rev. A **106**, 053322 (2022).
- [27] S. Li, U.N. Le and H. Saito, *Long-lifetime supersolid in a two-component dipolar bose-einstein condensate*, Phys. Rev. A **105**, L061302 (2022).
- [28] S. Saccani, S. Moroni and M. Boninsegni, *Phase diagram of soft-core bosons in two dimensions*, Phys. Rev. B **83**, 092506 (2011).
- [29] S. Saccani, S. Moroni and M. Boninsegni, *Excitation Spectrum of a Supersolid*, Phys. Rev. Lett. **108**, 175301 (2012).
- [30] F. Ancilotto, M. Rossi and F. Toigo, *Supersolid structure and excitation spectrum of soft-core bosons in three dimensions*, Phys. Rev. A **88**, 033618 (2013).
- [31] G. Pupillo, A. Micheli, M. Boninsegni, I. Lesanovsky and P. Zoller, *Strongly Correlated Gases of Rydberg-Dressed Atoms: Quantum and Classical Dynamics*, Phys. Rev. Lett. **104**, 223002 (2010).
- [32] N. Henkel, R. Nath and T. Pohl, *Three-Dimensional Roton Excitations and Supersolid Formation in Rydberg-Excited Bose-Einstein Condensates*, Phys. Rev. Lett. **104**, 195302 (2010).
- [33] M. N. Tengstrand, D. Bohlm, R. Sachdeva, J. Bengtsson and S. M. Reimann, *Persistent currents in toroidal dipolar supersolids*, Phys. Rev. A **103**, 013313 (2021).
- [34] R. Sachdeva, M.N. Tengstrand, and S.M. Reimann, *Self-bound supersolid stripe phase in binary Bose-Einstein condensates*, Phys. Rev. A **102**, 043304 (2020).
- [35] M.N. Tengstrand and S.M. Reimann, *Droplet-superfluid compounds in binary bosonic mixtures*, Phys. Rev. A **105**, 033319 (2022).
- [36] F. Ancilotto, M. Barranco and M. Pi, *Breakup of quantum liquid filaments into droplets*, Phys. Rev. A **107**, 063312 (2023).
- [37] Y. Ma, C. Peng and X. Cui, *Borromean Droplet in Three-Component Ultracold Bose Gases*, Phys. Rev. Lett. **127**, 043002 (2021).
- [38] Y. Ma and X. Cui, *Shell-shaped quantum droplet in a three-component ultracold Bose gas*, Phys. Rev. Lett. **134**, 043402 (2025).
- [39] F. Ancilotto, *Comment on “Shell-Shaped Quantum Droplet in a Three-Component Ultracold Bose Gas”*, Phys. Rev. Lett. **135**, 159301 (2025).
- [40] For the numerical evaluation of Eq. (2) it is convenient to use the following transformation
- $$\int_0^\infty g(k)dk = \int_0^{\pi/2} g[\tan(t)] \frac{dt}{\cos^2(t)} \quad (19)$$
- The right-hand side integral has been computed numerically using a Second Euler-McLaurin summation formula refined until some specified degree of accuracy is achieved [41].
- [41] W.H. Press, S.A. Teukolsky, W.T. Vetterling, and B.P. Flannery, *Numerical Recipes in Fortran 77: The Art of Scientific Computing*, 2nd. ed. (Cambridge University Press, New York, 1999).
- [42] A. Ralston and H. S. Wilf, *Mathematical methods for digital computers* (John Wiley and Sons, New York, 1960).
- [43] K. Mukherjee and S. M. Reimann, *Classical-linear-chain behavior from dipolar droplets to supersolids*, Phys. Rev. A **107**, 043319 (2023).
- [44] Y. Pomeau and S. Rica, *Dynamics of a model of a supersolid*, Phys. Rev. Lett. **72**, 2426 (1994).
- [45] N. Sepulveda, C. Josserand and S. Rica, *Superfluid density in a two-dimensional model of supersolid*, Eur. Phys. J. B **78**, 439–447 (2010).
- [46] L. Pitaevskii and S. Stringari, *Bose-Einstein Condensation and Superfluidity* (Oxford University Press, 2016).
- [47] M. Sindik, T. Zawislak, A. Recati and S. Stringari, *Sound, superfluidity, and layer compressibility in a ring dipolar supersolid*, Phys. Rev. Lett. **132**, 146001 (2024).
- [48] L. M. Platt, D. Baillie, and P. B. Blakie *Supersolid spectroscopy*, Phys. Rev. A **111**, 053305 (2025).
- [49] L. Tanzi, S.M. Rocuzzo, E. Lucioni, F. Fama', A. Fioretti, C. Gabbanini, G. Modugno, A. Recati and S. Stringari, *Supersolid symmetry breaking from compressional oscillations in a dipolar quantum gas*, Nature **574**, 382–385 (2019).
- [50] W. Kirkby, Au-Chen Lee, D. Baillie, T. Bland, F. Ferlaino, P.B. Blakie and R.N. Bisset, *Excitations of a Binary Dipolar Supersolid*, Phys. Rev. Lett. **133**, 103401 (2024).
- [51] M. Guo, F. Bottcher, J. Hertkorn, J-N. Schmidt, M. Wenzel, H.P. Buchler, T. Langen and T. Pfau, *The low-energy Goldstone mode in a trapped dipolar supersolid*, Nature **574**, 386 (2019).
- [52] G. Biagioni, N. Antolini, B. Donelli, L. Pezze', A. Smerzi, M. Fattori, A. Fioretti, C. Gabbanini, M. Inguscio, L. Tanzi and G. Modugno, *Measurement of the superfluid fraction of a supersolid by Josephson effect*, Nature **629**, 773 (2024).
- [53] A. Gallemí, S.M. Rocuzzo, S. Stringari, and A. Recati, *Dipolar Quantum Gases Quantized vortices in dipolar supersolid Bose-Einstein-condensed gases*, Phys. Rev. A **102**, 023322 (2020).